JAERI-Research
2001-056

DYNAMIC BEHAVIOR OF TRANSPORT IN NORMAL AND REVERSED SHEAR PLASMAS WITH INTERNAL BARRIERS IN JT-60U

December 2001

Sergi V. NEUDATCHIN*, Tomonori TAKIZUKA, Hiroshi SHIRAI,
Takaaki FUJITA, Akihiko ISAYAMA, Yutaka KAMADA,
Yoshihiko KOIDE and Yuri N. DNESTROVSKIJ*

日本原子力研究所
Japan Atomic Energy Research Institute

本レポートは、日本原子力研究所が不定期に公刊している研究報告書です。
入手の問合わせは、日本原子力研究所研究情報部研究情報課（〒319-1195　茨城県那珂郡東海村）あて、お申し越し下さい。なお、このほかに財団法人原子力弘済会資料センター（〒319-1195　茨城県那珂郡東海村日本原子力研究所内）で複写による実費頒布を行っております。

This report is issued irregularly.
Inquiries about availability of the reports should be addressed to Research Information Division, Department of Intellectual Resources, Japan Atomic Energy Research Institute, Tokai-mura, Naka-gun, Ibaraki-ken 〒319-1195, Japan.

編集兼発行　日本原子力研究所

JAERI－Research 2001－056

Dynamic Behavior of Transport in Normal and Reversed Shear Plasmas with Internal Barriers in JT-60U

Sergi V. NEUDATCHIN*, Tomonori TAKIZUKA, Hiroshi SHIRAI, Takaaki FUJITA, Akihiko ISAYAMA, Yutaka KAMADA, Yoshihiko KOIDE and Yuri N. DNESTROVSKIJ**

Department of Fusion Plasma Research
Naka Fusion Research Establishment
Japan Atomic Energy Research Institute
Naka-machi, Naka-gun, Ibaraki-ken

(Received November 13, 2001)

Transport evolution in normal shear (NrS) and reversed shear (RS) JT-60U tokamak plasmas with internal transport barrier (ITB) is described as a combination of various fast and slow time scale processes. Abrupt in time (ms time scale) and wide in space (~0.3 of minor radius) variations of electron and ion heat diffusivities $\chi_{e,i}$ ($\delta\chi_{e,i}$), which are called ITB-events and seen as simultaneous rise and decay of electron and ion temperatures in two spatial zones, are found for weak ITBs in both NrS and RS plasmas. Profiles of $\delta\chi_e$ in RS plasmas with strong ITBs are usually localized near ITB foot inside smaller space region. The maximum of the heat flux variation is located near position of the minimum of safety factor in various RS plasmas, and variation is extended in positive shear region. Inward and outward heat pulse propagations created by the jump of χ_e and the sawtooth-like crash are analyzed. Small values of χ_e and the absence of heat pinch are found inside strong ITBs. Another non-local abrupt variations of χ_e inside most of the plasma volume, including significant part of weak ITB inside RS zone of RS plasmas, are seen at the ELM-induced H-L transition and the L-H recovery.

Keywords: Tokamak, JT-60U, Normal Shear Plasma, Reversed Shear Plasma, Internal Transport Barrier, Trangient Transport Analysis, Heat Diffusivity, ITB-event, Heat Pulse Propergation, Non-local Transition, L-H Transition, H-L Transition

---

* Permanent position: Nuclear Fusion Institute, Russian Research Center "Kurchatov Institute"
** Nuclear Fusion Institute, Russian Research Center "Kurchatov Institute"

JT-60U 中の内部障壁を持つ正及び負シアプラズマにおける輸送の動的挙動

日本原子力研究所那珂研究所炉心プラズマ研究部
Sergi V. NEUDATCHIN*・滝塚　知典・白井　浩・藤田　隆明・諫山　明彦
鎌田　裕・小出　芳彦・Yuri N. DNESTROVSKIJ**

（2001年11月13日受理）

JT-60U トカマク中の内部輸送障壁(ITB)を持つ正及び負磁気シアプラズマにおける輸送の時間発展は、速い時間スケールの過程とゆっくりした時間スケールの過程との組み合わせで進む．正及び負磁気シアプラズマ中の弱いITBにおいて、時間的に急激で(ms時間スケール)空間的に広がりのある(小半径の0.3程度)変化が電子とイオンの熱拡散係数に生じることを見いだした．ITB事象と呼ばれるこの変動は、電子とイオン温度の2空間域で同時的に起きる増加と減小として観測される．強いITBを持つ負磁気シアプラズマ中では、熱拡散係数の変化分の空間分布は一般的にITBの足部近傍の狭い範囲に局在化する．様々な負磁気シアプラズマにおいて、安全係数がほぼ最小となるところで熱流束の変動が最大となる．またその変動の及ぶところは正シア領域まで拡がっている．熱拡散係数の急変及び鋸歯的崩壊によって誘起される内向きと外向きの熱パルス伝搬を解析し、強いITB領域内では熱拡散係数の値が小さくなっており熱ピンチはないことを確かめた．また、ELMで引起こされたH-L遷移時とその回復のL-H遷移時に同時発生する熱拡散係数の急激変動は、負磁気シアプラズマ中の弱いITB領域より内側の負シア領域まで含む広い範囲に亙って非局所的に起きることを見いだした．

那珂研究所：〒311-0193 茨城県那珂郡那珂町向山801-1
* 原所属：クルチャトフ研究所
** クルチャトフ研究所

Contents

目　次

This is a blank page.

1. Introduction

Over the past few years, a significant progress has been achieved in the development of the steady state Reversed magnetic Shear (RS) scenario [1,2] and steady state high-β_p scenario with Normal magnetic Shear (NrS) [3,4] in JT-60U plasmas with Internal Transport Barrier (ITB). Understanding properties of the ITB and identifying the control method of the ITB are among the most important issues for the tokamak fusion research. Processes of the transport evolution during RS and NrS discharges have not been fully understood yet. Characteristics of the ITB for RS plasmas and high-β_p NrS plasmas have been compared [5]. Two types of ITB, "parabolic" (weak ITB with large zone of reduced transport inside the ITB "foot") and "box" (strong ITB with very low transport between ITB "foot" and "shoulder") were observed, and transport properties for these cases have been analyzed [6]. The role of NBI toroidal momentum input for strong ITB sustainment was analyzed and the preference of the balanced momentum injection has been demonstrated [7]. The influence of the radial electric field calculated near ITB foot on wider ITB region was highlighted in Ref. [8].

Abrupt variations of ITB properties in RS JT-60U plasmas were reported in Refs. [9,10]. Recently, fast transient phenomena ("events") were studied in detail in RS plasmas with weak ITB [11]. Dipole T_e variation after an "event" (referred to as the "ITB-event" in the rest of the paper), or abrupt simultaneous rise and decay of T_e in two zones, was found. Dipole T_e variation is created by abrupt in time (ms time scale) and wide in space variation of electron heat diffusivity χ_e, $\delta\chi_e$, at the time of the ITB-event. ITB-events were described as spontaneous-like bifurcations of confinement. Spatial region of χ_e reduction (or increase) was wide in space (sometimes around 0.3 of the volume averaged minor radius a) and well extended into the zone of T_e decay (or rise). This spatial region was spread well into the positive shear space zone. Abrupt variations of χ_e were found earlier in NrS plasmas with ITB [10,12], but profiles of χ_e have not been obtained.

Usually, local heat fluxes are obtained from detailed power balance calculations. However, it is not easy to separate electron and ion heat fluxes from the total flux, especially in some of high performance regimes. Moreover, even the knowledge of heat diffusivities obtained from power balance, $\chi_{e,i}^{PB}$, in nearly steady-state conditions, is not sufficient to resolve the structure of the heat flux fully. This is because the problem of the existence of a "heat pinch" (or a large inward convective heat flux [13-15]) is not solved finally in tokamak plasmas. In this case values of $\chi_{e,i}^{PB}$ are not the real values of $\chi_{e,i}$, but are smaller values linked to the difference between large outward and inward heat fluxes. The value measured with various methods of Heat Pulse Propagation (HPP) analysis [13,16-20] is not the χ_e^{PB} value but $\chi_e^{HP} = -\delta\Gamma_e / (n_e \delta\nabla T_e)$, where χ_e^{HP} is dynamic electron heat diffusivity, $\delta\Gamma_e$ is

electron thermal flux perturbation, n_e is electron density and $\delta\nabla T_e$ is electron temperature gradient perturbation. For L-mode plasmas with central heating, χ_e^{HP} values (with typical values 1-10 m^2/s) are usually a few times greater than χ_e^{PB} values [13,16,19,20] (so called "enhanced HPP"). This difference can be explained by either the presence of "heat pinch" [13-15], or by nonlinear dependence of χ_e on ∇T_e [13-16]. The χ_e dependence on ∇T_e, however, does not affect the diffusive picture of HPP since it can be written as $\chi_e^{HP} = \chi_e^{PB} + (\partial\chi_e^{PB}/\partial\nabla T_e)\nabla T_e$ [13-16] (verified with transport code calculations in Refs. [14,16]). Low values of χ_e^{HP} and the absence of a significant "heat pinch" were found for some L-mode regimes with improved confinement on T-10 (inward HPP from off-axis ECRH swiching-on [21], and very slow outward HPP with $\chi_e^{HP} \sim 0.14 m^2/s$ induced by on-axis ECRH in a steady-state off-axis ECRH background plasma [22]) and on JET (inward HPP from off-axis ICRH in PEP-mode [23] and sawtooth-induced HPP in VH-mode [19,20] with $\chi_e^{HP} \sim 0.7 m^2/s$ for both cases). By our up to date information, the HPP was not studied inside the ITB region located inside RS zone of tokamak plasmas, while the HPP was recently studied inside the ITB formed by the series of ITB-events in positive shear zone of JT-60U RS plasmas [24].

Non-local ("global") plasma response was seen as simultaneous (ms time scale) temperature rise or decay in all plasma volume located outside ~0.3 of minor radius due to fast L-H-L transitions observed in some regimes on JT-60U [10,12,25] and JET [19,26,27]. This response was interpreted as abrupt jump of $\chi_{e,i}$ in the wide region. Non-local plasma response to peripheral $T_{e,i}$ perturbations (created e.g. by impurity laser blow-off) is sometimes also observed (see Ref. [28] and references therein). Plasma response to fast L-H-L transitions was not studied for RS plasmas.

The present paper represents expanded version of our report at 18th IAEA Fusion Energy Conference held in Sorrento [29]. The paper describes the behaviour of T_e and T_i after ITB-events in NrS plasmas. Profiles of χ_e variations for ITB-events in NrS and RS plasmas are evaluated and compared. The ITB-event induced HPP and the sawtooth-like crash induced HPP are analyzed inside the ITB located in the RS zone. Response of T_e located inside ITB to ELM-induced H-L transitions is also presented. Most of the results shown below were obtained by the analysis of the data from 12-channel high-space-resolution (1.7 cm half width and ~3 cm distance between channels for pulses analyzed below) electron cyclotron emission (ECE) heterodyne radiometer used for T_e measurements [30] (channel 1 is called below ch.1, etc.)

2. ITB-events in NrS and RS Plasmas

In this section, we first analyze ITB evolution in NrS 1.5MA/3.8T discharge E34487. Time traces of this NBI-heated discharge are shown in Fig. 1 with: the injected NB power P_{NB}; stored energy measured with diamagnetic loop, W_{dia} ; ion and electron temperatures, $T_{e,i}$, measured near $\rho \approx 0.4$ for ions and $\rho \approx 0.4$, 0.65 for electrons, where ρ denotes volume averaged minor radius normalized by the radius of a separatrix magnetic surface. More detailed evolution of T_e measured by heterodyne radiometer channels 5 ($\rho = 0.42$) and 12 ($\rho = 0.67$) is shown in Fig. 2. Radial profiles of T_i given by charge-exchange recombination spectroscopy measurements (circles), T_e by ECE Fourier-transformed spectroscopy measurements (squares) and n_e by YAG Thomson scattering measurements (triangles) just before t = 4.6s are shown in Fig. 3. We can briefly describe the plasma evolution shown in Figs. 1-2 as follows. Weak ITB is created before 4.6s because the ITB foot can be clearly observed on the T_i profile at t = 4.6s, shown in Fig. 3. The ITB event I (ITB-Improvement) has occurred at t = 4.602s, marked by the vertical line in Fig 1 and by the arrow in Fig. 2. The rise of $T_i(0.4)$ and "bipolar" perturbation of T_e (rise of $T_e(0.4)$ and decay of $T_e(0.65)$) are clearly observed in Fig. 1 and in Fig. 2 (highlighted by arrows with (+) and (-) signs in both figures). Two BLM-crashes (BLM; Barrier Localized Mode) [31] have occurred at t = 5.0 and 5.1s seen as abrupt reduction of T_e(ch.5) and increase of T_e(ch.12) in Fig. 2. The second ITB-event D (ITB-Degradation) is observed at t = 5.985s (70 ms after P_{NB} was switched-off) shown by the vertical line in Fig. 1 and by the arrow in Fig. 2. The ITB-event D is observed as simultaneous decay channel 5 and rise channel 12 of T_e (spatially inverse T_e perturbation in comparison with the ITB-event I) clearly seen on Fig. 2.

We now analyze the ITB-event I in detail. Profiles of $T_{e,i}$ 90 ms after the ITB-event are shown in Fig. 3 by solid lines. ITBs are either improved by ITB-events (negative $\delta\chi_e$) or degraded by them (positive $\delta\chi_e$). We may call this ITB-event as ITB "improvement" or, at the same time, formation of stronger ITB out of the weak one. Positions of radiometer channels 1 and 12 are marked in Fig. 3 by vertical dashed lines. The ITB-event I is seen as an abrupt rise of T_e observed at channels 1-7 and decay at channels 10-12 (discontinuous in time jump of $\partial T_e/\partial t$, $\delta(\partial T_e/\partial t)$, in ms time scale). Few ms delays of T_e(ch.8) rise and T_e(ch.9) decay are seen as not fully clear tendencies. The profile of $<\delta(\partial T_e/\partial t)>$ (brackets <> denote time averaged quantity during 10 ms time interval) is shown in Fig. 3.

The appearance of the discontinuous change of T_e is explained in Refs. [11,24] as a jump of χ_e in time across the ITB-event time $t = t_0$. It is changed abruptly at $t = t_0$ from χ_e to $\chi_e + \delta\chi_e$. The difference of transport equations between two phases after and before the ITB-event is given as

$$1.5\, n_e\, \delta(\partial T_e/\partial t) = \mathrm{div}\{n_e\, [\delta\chi_e \nabla T_e + (\chi_e + \delta\chi_e)\, \delta\nabla T_e]\}\ . \qquad (1)$$

In order to obtain the value of $\delta\chi_e$ from the measurement of $\delta(\partial T_e/\partial t)$, we integrate Eq. (1) over volume. Due to the limited measurement accuracy, we use time averaged values for $t_0 < t < t_0 + \Delta t$ instead of the instantaneous values just after $t = t_0$. In the present study an interval of $\Delta t =$ 10 ms is adopted for ITB-events I and D. The relation between $\delta\chi_e$ and $\delta(\partial T_e/\partial t)$ is expressed as

$$<\delta\chi_e> + <(\chi_e + \delta\chi_e)\, \delta\nabla T_e> / \nabla T_e = 1.5\, \{\int_0^{V(r)} n_e <\delta(\partial T_e/\partial t)>\, dV\} / \{n_e \nabla T_e\, A(r)\} \qquad (2)$$

where brackets <> denote time averaged quantity, A(r) is surface area of a magnetic surface at minor radius r, and V(r) is the volume surrounded by this surface. The second term on the left-hand side (LHS) of Eq. (2) originates from the diffusive spread of the perturbed temperature δT_e, whose weight in Eq. (2) is small unless Δt is small. Analytical estimates of this term's role can be found in Ref. [11], and numerical analysis of the diffusive spread of the $\delta\chi_e$ profile "measured" with Eq. (2) without the second term on the LHS is given in Ref. [24]. The influence of the abrupt change in the particle transport is not taken into account here; it was estimated analytically and numerically in Refs. [11,24] and has been shown not to influence $\delta\chi_e$ profile significantly. The profile of negative $\delta\chi_e$ for the ITB-event "I" without the second term on the LHS of Eq. (2) is shown in Fig. 5 by the dashed line with circles. The χ_e is reduced in a wide region (over 0.3a) and reaches the minimum value of $\delta\chi_e \approx -0.4$ m^2/s. The main case of the error in the estimation of $\delta\chi_e$ is usually the measurement error in ∇T_e (the denominator on the RHS of Eq. (2)). Neglecting the small role of second term on the LHS of Eq. (2) (for small Δt), Eq. (2) can be rewritten to give an estimate for the electron heat flux jump across magnetic surface A(r) :

$$<\delta\Gamma_e\, A> = -<\delta\chi_e> \{n_e\, \nabla T_e\, A(r)\} = -1.5\, \{\int_0^{V(r)} n_e <\delta(\partial T_e/\partial t)>\, dV \qquad (3)$$

The profile of $<\delta\Gamma_e\, A>$ for the ITB-event I obtained with Eq. (3) is shown by the dotted line in Fig. 4, the extremes of the $<\delta\Gamma_e\, A>$ error bars estimated from uncertainties in profiles of n_e and $<\delta(\partial T_e/\partial t)>$ are also shown. The χ_e decreases in the region of negative $<\delta(\partial T_e/\partial t)>$ because even on the outer edge of the 12th channel space half-width, the value of $<\delta\Gamma_e\, A>$ is negative (~50% of the minimum value -0.7 MW). The minimum of the $<\delta\Gamma_e\, A>$ is located near ITB

foot. The region of the χ_e decrease spreads well outside the ITB foot on T_i shown in Fig. 4 by the arrow. We can roughly estimate the jump of the ion heat flux $<\delta\Gamma_i\ A>$ in order to compare $<\delta\Gamma_e>$ and $<\delta\Gamma_i>$. The values of $<\delta(\partial T_i/\partial t)>$ taken from experiment (~7cm space and 17 ms time resolution) are nearly 3.5 times higher in comparison with $<\delta(\partial T_e/\partial t)>$ values. The minimum value of $<\delta\Gamma_i\ A>$ is estimated as ~1.2MW. Power balance calculations are performed with 1.5 dimensional transport code TOPICS (TOkamak Prediction and Interpretation Code System) [32]. The NBI power deposition to electrons and ions is calculated by OFMC (Orbit Following Monte-Carlo) code [33], which takes into account ripple loss, banana orbit loss and charge exchange loss of slowing-down fast ions. The absorbed 4.8MW power is found inside r=0.45 with nearly 40% level of the convective heat losses. The similar level of the convective heat losses (~50%) was measured for ρ = 0.35 in the other pulse with the new method suggested in reference [34]. The total diffusive heat flux by electron and ion channels equal to 2.9 MW (the rest ~60% part of 4.8MW) is found at ρ = 0.45 (separate electron and ion diffusive heat fluxes are known with larger errors), while $<\delta\Gamma_i\ A> + <\delta\Gamma_e\ A> \approx$ -1.9MW at the same ρ = 0.45. The total diffusive heat flux by electron and ion channels is reduced as much as ~3 times at the ITB-event I.

For the second ITB-event D (ITB-degradation) observed at t = 5.985s, profiles of $<\delta(\partial T_e/\partial t)>$ and $\delta\chi_e$ are inverted in comparison with the ITB-event I. The profile of positive $\delta\chi_e$ calculated without the second term on the LHS of Eq. (2) is shown in Fig. 5 by the dashed line. Increase of χ_e in a wide region (over 0.3a) and the maximum value of $\delta\chi_e \approx 0.4\ m^2/s$ are seen similarly to $\delta\chi_e$ features at the ITB-event I.

The negative profile of $\delta\chi_e$ obtained for the ITB-event in RS pulse 32423 with weak ITB (see Fig. 5 in Ref. [11]) is shown by squares in Fig. 5. Spatial positions of channels 1-12 are taken from 0.37 to 0.66 of minor radius in RS and from 0.29 to 0.67 in NrS plasmas. Profiles of $\delta\chi_e$ are similarly wide (around 0.3a) for ITB-events in NrS and RS plasmas with weak ITBs, while MSE-measured q profiles shown in Fig. 5 are very different. Profiles of $\delta\chi_e$ are similarly expanded outside of ITB-foots in the both NrS and RS cases.

Widths of strong ITBs in RS JT-60U plasmas are usually smaller (0.1-0.15a) in comparison with weak ITB widths (sometimes over 0.4a). Profiles of T_e just before (time A, t = 5.735s) and 15 ms after the ITB-event in RS 1.5MA/3.8T discharge E32424 with strong ITB (P_{NB} = 10.5MW, W = 2.8MJ, τ_E ~ 0.25s) are shown in Fig. 6 by solid and dashed curves, respectively. The ITB shoulder is observed near the location of radiometer channel 4 and ITB foot is seen near the position of channel 8 in Fig. 6. Profiles of T_i (circles), n_e (triangles) and MSE-measured q (dashed line) just before the ITB-event are shown in Fig. 7. The ITB shoulder and foot are observed on T_i profile also. Positions of radiometer channels 1 and 12 are marked in Fig. 7 by vertical dashed lines. The ITB-event "improvement" is seen as T_e rise

in small region (initially on channels 7 and 8 as marked in Fig. 6) and decay on channels 11 and 12. The profile of $\delta\chi_e$ shown in Fig. 6 (dotted curve, calculated as described above) is localized near ITB foot, compared with spatially wider $\delta\chi_e$ profiles in weak ITB cases, and extended into positive shear region (at least slightly outside channel 12, well above the error bars). The minimum value of $<\Gamma_e A> \approx -1$MW is obtained with Eq. (3) and is located near the ITB foot. Values of $\delta\chi_e$ are inversely proportional to ∇T_e, while ∇T_e itself is not well-known in the region outside q_{min} where ∇T_e is small. Gradual diffusive broadening of rising positive T_e perturbation δT_e is observed later in time (region of inward electron HPP is shown by the arrow marked "HPP" in both Figs. 6 and 7 and is analyzed in Section 3 below.

3. Inward and Outward Heat Pulse Propagation inside ITB in RS

New sources of Heat Pulse Propagation (HPP) are found in RS plasmas. We now analyze the outward HPP created by a source observed as sawtooth-like crash in central part of RS plasmas. Time traces of 1.8MA/3.7T RS shot E36614 are shown in Fig. 8, where P_{NB} is the NB power, P_{EC} is the injected ECRH power (see details of recently installed ECRH system in Ref. [35]); W is the stored energy and T_e was measured by radiometer channels 1,9,12 at ρ = 0.3, 0.53, 0.62, respectively. At the time of the crash highlighted by the arrow, the decay of T_e(ch.1) and the rise of T_e(ch.9) can be seen. Profiles of T_e before and after the crash (under P_{NB} = 5.4MW, P_{EC} = 1.2MW, W = 3.2MJ, $\tau_E \sim 0.5$ s) are shown in Fig. 9 by solid and dashed curves, respectively. Profiles of T_i (circles), n_e (triangles) and MSE-measured q (dashed line) just before the crash are shown in Fig. 10, locations of radiometer channels 1 and 12 are marked by dashed vertical lines. Time traces of T_e(ch.9-12) are shown in Fig. 11, crash-induced T_e rise is observed on ch.9 and ch.10. Since no clear response on channel 11 is observed, one cannot obtain the χ_e^{HP} value but can only estimate its upper limit.

Regarding perturbations of heat sources and n_e, the HPP is analyzed with a simplified transport equation for δT_e, as usual,

$$1.5\, n_e\, \partial\delta T_e/\partial t = \mathrm{div}(n_e\, \chi_e^{HP}\, \nabla\delta T_e), \quad r_{10} \le r \le r_{sep} \tag{4}$$

with zero initial condition $\delta T_e(r,t=0) = 0$. Left boundary condition $\delta T_e(r_{10},t)$ is taken from experimental measurements at the ch.10 position $r = r_{10}$; $\delta T_{e,CALC}(r_{10},t) = \delta T_{e,EXP}(r_{10},t)$ similarly to that used in Refs. [17,18]. Right boundary condition is chosen as zero at the separatrix radius $r = r_{sep}$; $\delta T_{e,CALC}(r_{sep},t) = 0$. The $n_e(r)$ profile is taken from the experiment. Calculated δT_e at positions of ch.11 ($r=r_{11}$) and ch.12 ($r=r_{12}$), $\delta T_{e,CALC}(r_{11,12},t)$, depends

on χ_e^{HP}, i.e., $\delta T_{e,CALC}(r_{11,12},t) = \delta T_{e,CALC}(\chi_e^{HP},r_{11,12},t)$. Equation (4) is solved in a cylindrical geometry (positions of $r_{10\text{-}12}$ are taken as volume averaged minor radii from JT-60U equilibria with measured q-profiles), using implicit conservative difference scheme described in Ref. [36]. The difference problem is solved with a three point Gauss eliminating method described for example in Ref. [36].

One experimental important characteristic of the HPP, the index of "quality" of a heat wave, was introduced in Refs. [19,20]. The index reflects the "relative sharpness" of the heat wave. It was defined as

$$S = |(\delta\nabla T_e/\delta T_e)/(\nabla T_e/T_e)| \ . \qquad (5)$$

This is the experimental characterization of the sensitivity of the conduction term ($\chi_e^{HP}\delta\nabla T_e$) to terms proportional to δT_e, such as convective (perturbation of convective heat flux) and "convective-like" terms (source perturbation, gradual dependencies of χ_e on time and T_e, etc.). Generally, the value of S decreases in time due to a diffusive spread of δT_e, as the space region of high S values moves outward. This is one of the reasons why the HPP study is bounded in time. The HPP with high values of $S > 5$ are studied in all cases reported in the present paper. These values should be treated as high because values of S for sawteeth induced HPP study on JET were usually equal to 2 or 3 [19,20].

The upper limit of χ_e^{HP} is estimated as follows. The time trace of the $\delta T_{e,EXP}$ at r_{10} is shown in Fig. 12 by the solid line. The evolutions of $\delta T_{e,CALC}(r_{11})$ obtained with $\chi_e^{HP} = 0.1m^2/s$ (amplitude at $t = t_{CRASH} + 15ms$ shown by double-sides arrow) and $\chi_e^{HP} = 0.04m^2/s$ are shown by dashed lines. The magnitude of $\delta T_{e,CALC}(r_{11},t_{CRASH}+15ms)$ obtained with $\chi_e^{HP} = 0.1m^2/s$ is shown in Fig. 11 by the solid vertical gray short segment with the amplitude above error bars of the gradual $T_e(r_{11},t)$ evolution. The value of $\delta T_{e,CALC}(r_{11}, t = t_{CRASH} + 15\ ms)$ derived with $\chi_e^{HP} = 0.04m^2/s$ is reduced by ~2 times in comparison with the one derived with $\chi_e^{HP} = 0.1m^2/s$. The HPP with $\chi_e^{HP} = 0.04m^2/s$ probably could not be recognized easily. The upper limit $\chi_e^{HP} = 0.06m^2/s$ is obtained as the result of a compromise between calculations with $\chi_e^{HP} = 0.1m^2/s$ (should be seen easily in the experiment) and calculations with $\chi_e^{HP} = 0.04m^2/s$ (probably not easily seen). Other possible explanations of the absence of HPP (temperature and density coupled transport, perturbation of energy sources at the crash, etc.) could not be fully rejected at present. However, very slow HPP is also seen (preliminary analysis) in the case of the outward ECRH-induced HPP (without abrupt perturbations of n_e and T_i) throughout ITB in similar shots. This preliminary result strongly supports the view that very low values of χ_e^{HP} are particularly responsible for HPP with $\chi_e^{HP} < 0.06m^2/s$ described above. The value of the ion neoclassical heat diffusivity $\chi_i^{neo} = 0.3m^2/s$

is calculated in the region of HPP with code [37] and with expressions described in Ref. [38], i.e. $\chi_e^{HP} < 0.2\ \chi_i^{neo}$ for this case.

The ITB-event induced the inward electron HPP is found inside strong ITB in the RS region in shot 32424, indicated by the arrow marked "HPP" in Fig. 6. The evolution of T_e (ch.6,5) is shown in Fig. 13, the time of the ITB-event is marked by the symbol A, 15 ms later time marked by the symbol B. A few ms time delay in the rise of T_e(ch.6) is clearly observed (the rise has started at time A somewhere between channels 6 and 7). The inward HPP from channel 6 to channel 5 is schematically shown by the arrow in Fig. 13. The HPP is analyzed with numerical solution equation (4) solved in the region $0 \le r \le r_6$ with zero initial condition, the right boundary condition $\delta T_{e,CALC}(r_6,t) = \delta T_{e,EXP}(r_6,t)$ being taken from experiment and with left boundary condition $\partial \delta T_e(0,t)/\partial r = 0$. The calculated amplitude of δT_e(ch.5) with χ_e^{HP} = 0.2 m^2/s (26ms after time A) is shown by the bold segment. The value of $\chi_e^{HP} = 0.12\ m^2/s \approx 0.5\ \chi_i^{neo}$ is found from the best fit of the calculated and experimental data on channel 5 (with approximately -40% and +50% errorbars).

Formation of a strong ITB in positive shear zone of RS plasmas (shot E32423) is described as a series of 3 consecutive ITB-events [24]. Evolution of δT_e (induced by the third ITB-event) is observed as the outward HPP from radiometer channel 9 (left boundary condition for calculations as was described above for shot 36614) to channels 10,11 (throughout the region with ITB-event improved confinement) and is shown in Fig. 14 by solid (experiment), dashed ($\delta T_{e,CALC}(r_{10},t)$ and $\delta T_{e,CALC}(r_{11},t)$ with $\chi_e^{HP} = 0.1 m^2/s$) and dotted lines ($\delta T_{e,CALC}(r_{11},t)$ with χ_e^{HP} =0.2 and 0.05 m^2/s). Values of $\chi_{e,i}^{HP}$ as low as ~$0.1 m^2/s$ are obtained from electron and ion HPP (see details in Ref. [24]) in the ~8cm wide region fully localized in positive shear space zone of RS plasmas. Similar value of the ion neoclassical heat diffusivity $\chi_i^{neo} \approx 0.1\ m^2/s$ is calculated in the same space region.

Real χ_e in the plasma is equal to χ_e measured with power balance χ_e^{PB} under any dependence of χ_e on plasma parameters, except for the one with the presence of the heat pinch. For the "simple heat pinch" case, electron heat flux Γ_e is described by the expression $\Gamma_e = -n_e (\chi_e \nabla T_e + V_{Te} T_e)$, where V_{Te} is inward heat pinch velocity, $\delta\Gamma_e = -n_e (\chi_e \delta\nabla T_e + V_{Te} \delta T_e)$, when χ_e and V_{Te} are not varied during HPP. The value of $\chi_e^{PB} \equiv -\Gamma_e/(n_e \nabla T_e)$ in this case is not equal, but smaller than χ_e. The upper limit of V_{Te} (in the extreme case of overestimated V_{Te} with $\chi_e \nabla T_e + V_{Te} T_e = 0$ and $\chi_e^{PB} = 0$, see details in Ref. [24]) is equal to

$$V_{Te,upper} = -\chi_e^{HP} (\nabla T_e / T_e)/(1 - 1/S) \qquad (6)$$

with $V_{Te,upper}$ nearly independent from values of S for S >> 1 (heat wave sharpness, see Eq. (5)). The cases of HPP with high values of S > 5 are studied above. The values of $V_{Te,upper}$

estimated from Eq. (6) are found to be around or below 0.5m/s in all cases of HPP described in the present paper.

4. ITB Response to ELM-induced H-L Transitions in RS

The ways to obtain L-H transition in RS JT-60U plasmas are described in Ref. [1]. Time traces of the late phase of NBI-heated 1.5MA/3.8T discharge 32419 (weak ITB phase) are shown in Fig. 15, together with P_{NB}, W and divertor H_α. Many ELMs with post-ELM enhanced H_α level (~5-100 ms duration in various pulses) are clearly observed in Fig. 15. We analyze plasma response to the ELM labeled by the arrow marked t_1 in Fig. 15 in detail. Profiles of T_i (circles), n_e (triangles) and q (obtained from MSE measurements and shown by dotted line) before $t = t_1$ are shown in Fig 16. Weak ITB is clearly observed on T_i and n_e profiles. Location of radiometer channels 1 and 12 (r/a = 0.29 and 0.69) is marked by vertical dashed lines. Radial position of channel 1 is located well inside ITB and also inside RS region.

Time traces of W, H_α and T_e(ch.1) around the ELM at $t = t_1$ are shown in Fig. 17. ELM-induced H-L back transition is observed on the H_a trace shown in Fig. 17 as a post-ELM level enhanced by ~3 times in comparison with the pre-ELM one. Around 7% of energy is lost during the ELM-induced L-mode phase. The transition is observed as abrupt and simultaneous nearly linear decay of T_e inside ITB (ch.1-7), shown for channel 1 in Fig. 17. Decay of T_e is well correlated (~ 2 ms) with abrupt rise of H_α. The similar T_e behaviour is observed for ELMs before $t = t_1$. Profiles of T_e before and 10 ms after transition are shown in Fig. 18. The zone shown in Fig. 18 is located in RS region. The $\delta\chi_{e,H\text{-}L}$ profile obtained from Eq. (2) (with $<\delta(\partial T_e/\partial t)>$ values averaged in 10 ms time interval) is shown on Fig. 18 by circles. Small 25% correction (upper limit decrease of $|\delta\chi_{e,H\text{-}L}|$) because of inward plasma motion due to energy losses is introduced in calculations. The same role of plasma motion is obtained from T_e decay measured from low and high field side by ECE grating polychrometer, and by radiometer from low field side in another shot. An alternative explanation is that the decay of T_e is caused by the inward HPP from the ITB foot. Decay of T_e(ch.1-6) can be explained (still with some delay and slightly lower amplitude of δT_e(ch.1-3)) by the inward HPP from channel 7 calculated with $\chi_e^{HP} \sim 10 m^2/s$ (order of amplitude above typical χ_e^{PB} values obtained from power balance). A significant part of weak ITB located in RS zone is covered by abrupt increase of χ_e.

The similar picture is seen for L-H transition (H-mode recovery), observed in Fig. 17 as the disappearance of T_e decay correlated (within few ms) with the H_α decay. The corresponding profile of $\delta\chi_{e,L\text{-}H}$ (calculated similarly to the one described above for H-L transition) is inverted in comparison with H-L case and $\delta\chi_{e,L\text{-}H} \cong -\delta\chi_{e,H\text{-}L}$.

Response of strong ITB to ELM-induced H-L transitions is not fully clear at present. The region of T_e decay induced by irregularly observed ELM-like phenomena (with H_α level enhanced by ~50% for 5-10 ms) is limited by ITB foot and T_e decay does not penetrate inside ITB region. We are not sure whether this enhanced H_α level can be qualified as L-mode because in ELMs-induced L-modes H_α level is typically enhanced by 2-3 times.

5. Discussion

By our knowledge of T-10, JET and JT-60U data analyzed in Refs. [19-24] and in the present paper, small values of inward convective heat velocity of order of 0.5 m/s could be considered within the uncertainty of experiment in all regimes with improved electron confinement studied so far. These results are in contrast to the values of "heat pinch velocity" around 60 m/s claimed recently for the ECRH induced HPP throughout ITBs formed near rational q surfaces in RTP [39]. The presence or absence of the heat pinch in L-mode plasmas with on-axis heating is not clear yet. Some of JT-60U RS discharges with ITB were described by a "canonical profile" (CPTM) model [40], where L-mode confinement is formed by nearly balanced large inward convective and outward diffusive heat fluxes. The ITB is created due to "forgetting" of canonical profiles under some conditions in CPTM model, and heat pinch is absent inside ITB.

A more systematic analysis of ITB-events in NrS and RS plasmas is necessary to understand possible relationship of local measurable plasma parameters and ITB-events. The physical mechanism of ITB-events remains unclear.

The global nature of abrupt χ_e variations inside RS region reported in the present paper, is similar to abrupt variations of $\chi_{e,i}$ in 90% of plasma volume seen under "fast" L-H-L transitions in some JT-60U [25] and JET [19,26,27] NrS regimes without clear ITB including ELM-induced short (few ms) L-modes on JET (first time described in JET VH-mode plasmas [26]) and ELM-induced L-modes on JT-60U [26], and inside weak ITB in NrS JT-60U plasmas [10,12].

6. Conclusions

Abrupt in time (ms time scale) and wide in space (~0.3-0.4 of minor radius) variations of χ_e (ITB-events) are found in NrS high β_p plasmas with weak ITB. ITB-events are seen as "bipolar" perturbation of $T_{e,i}$ with simultaneous rise and decay of $T_{e,i}$ in two spatial zones. The maximum of the heat flux abrupt variation is located near ITB foot and the profiles of χ_e

variations $\delta\chi_e$ are extended well outside of ITB foot. Similar profiles of $|\delta\chi_e|$ are obtained for the both cases of ITB-improvement via ITB-event (negative $\delta\chi_e$) and ITB-degradation via ITB-event (positive $\delta\chi_e$). Widths of ITB-events are generally similar for weak ITBs in RS and NrS plasmas. The jump of the total heat flux by electron and ion channels is estimated for the case of ITB-improvement via ITB-event and compared with the results of power balance calculations before the ITB-event. The total diffusive heat flux is reduced by ~3 times at the ITB-event.

Profiles of $\delta\chi_e$ at the ITB-event in RS plasmas with strong ITB are localized near ITB foot in narrower region in comparison with wider $\delta\chi_e$ profiles in weak ITB case. In various RS pulses studied up to now, the maximum of the heat flux abrupt variation is always located near position of q_{min} and heat flux variation is always extended into positive shear region. In general, ITB-events are the intrinsic feature of various NrS and RS JT-60U plasmas. The space-time behaviour of T_i at ITB-events is similar to that of T_e in the both cases of NrS (present paper) and RS plasmas [11,24].

New sources of HPP are found in RS plasmas. The HPP is studied in RS zone of tokamak plasmas for the first time. We observe symmetric picture of slow HPP ($\chi_e^{HP} \approx 0.1 m^2/s$) in 3 cases: the ITB-event induced electron inward HPP ($\chi_e^{HP} \approx 0.5\,\chi_i^{neo}$) and the sawtooth-like crash induced outward HPP ($\chi_e^{HP} < 0.2\,\chi_i^{neo}$), both propagated throughout strong ITB in RS zone; the ITB-event induced electron and ion outward HPP ($\chi_e^{HP} \approx \chi_i^{HP} \approx \chi_i^{neo}$) throughout strong ITB abruptly formed by ITB-event in positive shear zone of RS plasmas (this case is described in Ref. [24] in detail). An important consequence of HPP analysis is the absence of electron and ion "heat pinch" in ITB region. Small values of inward convective heat velocity (near 0.5 m/s) could be considered within the uncertainty of experiment.

Fast response of T_e to ELM-induced H-L back transitions (seen as T_e decay correlated within 2 ms with abrupt rise of H_α) is found well inside weak ITBs in RS region, suggesting edge-core interplay across q_{min} on the ms timescale. The T_e decay is interpreted as abrupt appearance of positive $\delta\chi_e$. The similar behaviour is seen at H-mode recovery after ELM-induced L-mode, when abrupt appearance of negative $\delta\chi_e$ is correlated within few ms with decay of H_α. This is the first study of ITB fast response to L-H-L transitions in RS tokamak plasmas. In our latest report [41], we study this issue more systematically. The global nature of abrupt χ_e variations inside RS region is similar to χ_e behaviour at global L-H-L transitions in JT-60U [10,12,25] and JET [19,26,27] NrS plasmas.

Complex transport evolution inside ITB has been partially described in the present paper as highly dynamic system with variety of coupled processes. It is the mixture of fast time-scale processes (abrupt bifurcations of core transport due to "semi-global" ITB-events and fast edge-core connection throughout RS zone at global bifurcations of confinement during L-H-L

transitions) described in the present paper, and slow time scale processes (HPP and gradual variations of the confinement, strong linkage of current and pressure profiles in RS plasmas [1]). Moreover, the interplay between ITB-events and L-H transitions is also possible, as shown in our latest report [41]. The "semi-empirical" methods for plasma parameters control in RS and NrS discharges with ITB developed on JT-60U [1-8] are the only ones available at present to make progress in steady state RS and high β_p NrS discharges with ITB.

Acknowledgments

The authors thank Drs. T. Fukuda, S. Ide, S. Takeji and many other members of JT-60 team for their fruitful discussion and fine collaboration. They also are indebted to Drs. M. Azumi, M. Kikuchi, A. Kitsunezaki, H. Ninomiya, T. Ozeki and R. Yoshino for their continuous encouragements. This work was carried out during SVN's stay at JAERI under JAERI Research Fellowship.

References

[1] FUJITA, T., KAMADA, Y., ISHIDA, S., et al., Nucl. Fusion **39** (1999) 1627.

[2] FUJITA, T., et al., 18th IAEA Fusion Energy Conference (Sorrento, 2000) IAEA-CN77/EX4/1, to be published in Nucl. Fusion.

[3] KAMADA, Y., ISAYAMA, A., OIKAWA, T., et al., Nucl. Fusion **39** (1999) 1680.

[4] KAMADA, Y., et al., 18th IAEA Fusion Energy Conference (Sorrento, 2000) IAEA-CN77/OV1/1, to be published in Nucl. Fusion.

[5] KOIDE, Y., MORI, M., FUJITA, T., SHIRAI, H., et al., Plasma Phys. Control Fusion **40** (1998) 641.

[6] SHIRAI, H., KIKUCHI, M., TAKIZUKA, T., et al., Nucl. Fusion **39** (1999) 1713.

[7] SHIRAI, H., KIKUCHI, M., TAKIZUKA, T., et al., Plasma Phys. Control Fusion **42** (2000) A109.

[8] SAKAMOTO, Y., KAMADA, Y., IDE, S., et al., Nucl. Fusion **41** (2001) 865.

[9] FUJITA, T., IDE, H., KIMURA, S. et al., 16th IAEA Fusion Energy Conf. (Montreal, 1996) Vol. 1 (IAEA, Vienna, 1997) 227.

[10] NEUDATCHIN, S.V., TAKIZUKA, T., SHIRAI, H., FUJITA, T., TAKEJI, S., ISEI, N., KAMADA, Y., "Analysis of Space-Time Structure of Internal Transport Barrier in JT-60U" (1997) JAERI-Research 97-052.

[11] NEUDATCHIN, S.V., TAKIZUKA, T., SHIRAI, H., FUJITA, T., ISEI, N., ISAYAMA, A., KOIDE, Y., KAMADA, Y., Plasma Phys. Control. Fusion **41** (1999) L39.

[12] NEUDATCHIN, S.V., et al., Proc. 24th EPS Conf. on Control. Fusion and Plasma Phys., (Berchtesgaden, 1997), vol. 21A (EPS, Geneva, 1997), part II, p. 497.

[13] FREDRIKSON E.D., et al., Nucl. Fusion **26** (1986) 849.

[14] NEUDATCHIN, S.V., "Influence of Electron Temperature Perturbations on Electron Heat Diffusivity in a Tokamak" in: "Voprosy Atomnoi Nauki i Tekniki" (Questions of Atomic Science and Engineering, Thermonuclear Fusion Series) issue 3 (1986) p 39 (in Russian).

[15] CALLEN, J.D., et al., Nucl. Fusion **27** (1987) 1857.

[16] BAGDASAROV, A.A., VASIN, N.L., ESIPCHYK, Yu.V., NEUDATCHIN, S.V., RAZUMOVA, K.A., SAVRUKHIN, P.V. and TARASYAN, K.N., Soviet J. Plasma Phys. **13** (1987) 517.

[17] NEUDATCHIN, S.V., Proc. 15th EPS Conf. on Contr. Fusion and Plasma Heating (Dubrovnik, 1988) Vol. 12B (EPS, Geneva, 1988), part III, p. 1147.

[18] RIEDEL, K., et al., Nucl. Fusion **28** (1988) 1509.

[19] NEUDATCHIN, S.V., CORDEY, J.G., and MUIR, D.J., Proc. 20th EPS Conf. on Control. Fusion and Plasma Phys. (Lisboa, 1993) Vol.I (EPS, Geneva, 1993) p. 83.

[20] NEUDATCHIN, S.V. and MUIR, D.J., "The Study of Electron Heat Transport in JET by Analysing the Decay of Temperature Perturbations Induced by Sawteeth" JET Rep. JET-P(93)-27 (1993), Jet Joint Undertaking, Abingdon, Oxfordshire, UK.

[21] ALIKAEV, V.V., et al., Plasma Physics and Controlled Nuclear Fusion Research (Proc. 11th Int. Conf., Kyoto, 1986) Vol.1 (IAEA, Vienna, 1987) 111.

[22] BAGDASAROV, A.A., VASIN, N.L., NEUDATCHIN, S.V., SAVRUKHIN, P.V., Plasma Physics and Controlled Nuclear Fusion Research (Proc. 15th Int. Conf., Washington, 1990), Vol. 1 (IAEA, Vienna, 1991) 253.

[23] BALET, B., BOUCHER D., CORDEY, J.G., MUIR, D.J., NEUDATCIN, S.V., SHMIDT, G., Proc. 19th EPS Conf. on Control. Fusion and Plasma Phys. (Innsbruk, 1992) Vol. 16C (EPS, Geneva, 1992) part 1, p. 59.

[24] NEUDATCHIN, S.V., TAKIZUKA, T., SHIRAI, H., FUJITA, T., ISAYAMA, A., KOIDE, Y. and KAMADA, Y., Plasma Phys. Control. Fusion **43** (2001) 661.

[25] NEUDATCHIN, S.V., TAKIZUKA, T., SHIRAI, H., ISEI, N., KAMADA, Y., KOIDE, Y., SATO, M., AZUMI, M., Japan J. Appl. Phys. **35** (1996) 3595.

[26] NEUDATCHIN, S.V., CORDEY, J.G., and MUIR, D.J., "The Time Behaviour of the Electron Heat Conductivity during L-H and H-L Transitions in JET" JET Rep. JET-P (93)-58 (1993) Jet Joint Undertaking, Abingdon, Oxfordshire, UK.

[27] CORDEY, J.G., MUIR, D.J., NEUDATCHIN, S.V., et al., Plasma Phys. Control. Fusion **36** (1994) A267.

[28] CALLEN J.D., and KISSIK, M.W., Plasma Phys. Control. Fusion **39** (1997) 173.

[29] NEUDATCHIN, S.V., TAKIZUKA, T., SHIRAI, H., et al., Fusion Energy 2000 (Proc 18th IAEA Fusion Energy Conference, Sorrento 2000) CD-ROM C&S Papers Series 8/C (IAEA, Vienna, 2001) file EXP5/01.

[30] ISEI, N., et al., Rev. Sci. Instrum. **66** (1995) 413.

[31] TAKEJI, S., KAMADA, Y., OZEKI, T., et al., Phys. Plasmas **4** (1997) 4283.

[32] SHIRAI, H., TAKIZUKA, T., KOIDE, Y., et al., Plasma Phys. Control. Fusion **42** (2000) 1193.

[33] TANI, K., AZUMI, M., KISHIMOTO, H., TAMURA, S., J. Phys. Soc. Japan **64** (1981) 4209.

[34] POLEVOI, A.R., NEUDATCHIN, S.V., SHIRAI, H., TAKIZUKA, T., Japan J. Appl. Phys. **37** (1998) 671.

[35] IKEDA, Y., IDE, S., SUZUKI, T., et al., 18th IAEA Fusion Energy Conference (Sorrento, 2000) IAEA- CN77/EXP4/3, submitted to Nucl. Fusion.

[36] DNESTROVSKIJ, Yu.N., and KOSTOMAROV, D.P., "Numerical Simulation of Plasmas", Springer-Verlag (1986) p. 233.

[37] SHIRAI, H., TAKIZUKA T., NAITO O., et al., J. Phys. Soc. Japan **64** (1995) 4209.

[38] KIKUCHI, M., SHIRAI, H., ITAKURA, H., AZUMI, M., "Effect of Impurity on Neoclassical Ion Thermal Diffusivity", in "Review of JT-60U Experimental Results in 1997", JAERI-Research 98-039 (1998) p.43.

[39] MANTICA, P., et al., Proc. 26th EPS Conf. on Controlled Fusion and Plasma Physics (Maastricht, 1999) ECA Vol. 23J (EPS, Geneva, 1999) p. 1109.

[40] DNESTROVSKIJ, Yu.N., LYSENKO, S.E., TARASYAN, K.N., POLEVOI, A.R., SHIRAI H, TAKIZUKA, T. and KIKUCHI, M., Nucl. Fusion **39** (1999) 2089.

[41] NEUDATCHIN, S.V., TAKIZUKA, T., SHIRAI, H., FUJITA, T., ISAYAMA, A., KAMADA, Y., KOIDE, Y., SUZUKI, T. and TAKEJI, S. "Dynamics and Interplay of L-H-L Transitions and ITB-events in Reversed Shear Plasmas with Internal Barriers in JT-60U" 8th IAEA TCM on H-mode Physics and Transport Barriers, 2001 (Tajimi, Japan), submitted to Plasma Phys. Control. Fusion.

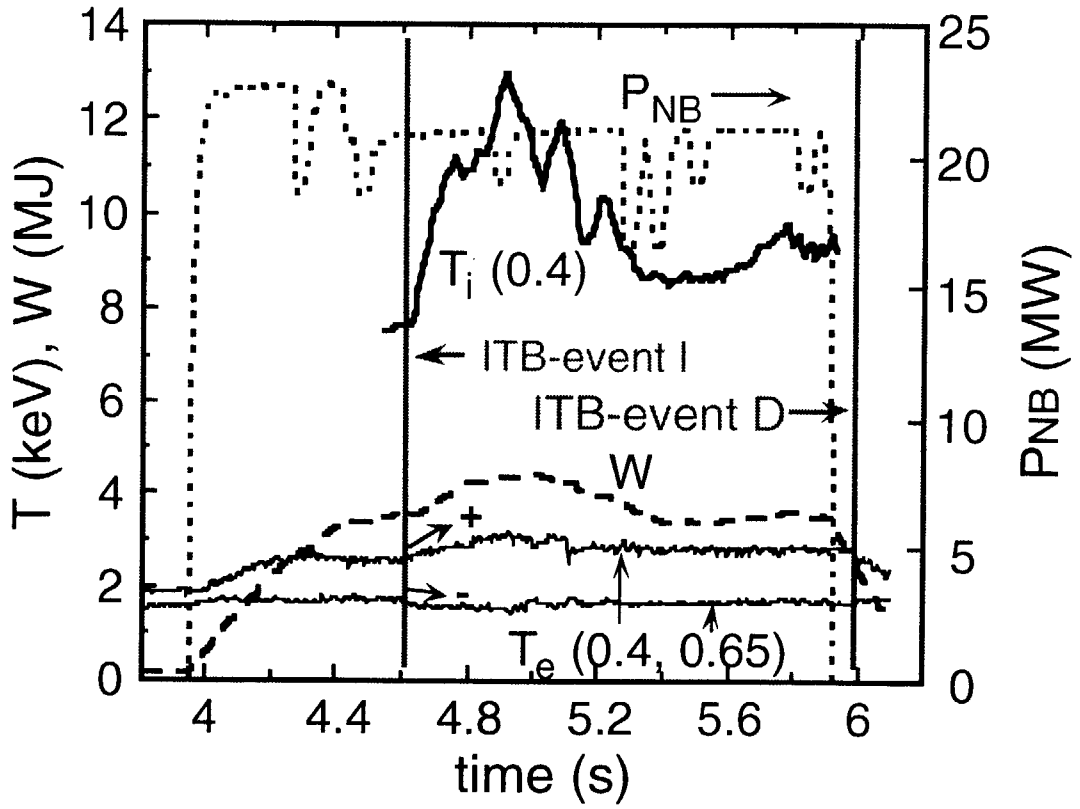

Fig. 1 Evolutions of T_i, T_e, W and P_{NB} for an NrS discharge 34487. Temperatures are measured near ρ = 0.4 for ions and ρ = 0.4, 0.65 for electrons. ITB events I (ITB-improvement) and D (ITB-degradation) occurs at times represented by vertical solid lines. "Bipolar" perturbation of T_e after ITB-event I is highlighted by arrows with signs (+) and (-).

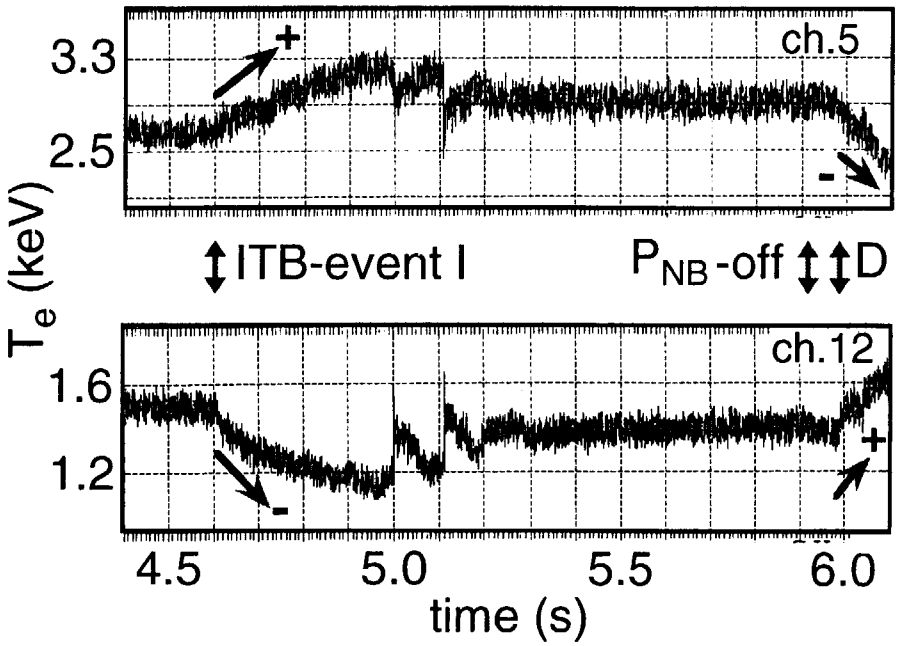

Fig. 2 Evolutions of T_e on heterodyne radiometer channel 5 (ρ = 0.42) and channel 12 (ρ = 0.67). ITB-events I, D and P_{NB} cut-off occurs at times shown by the double-side arrows. Two BLM-crashes (barrier localized mode) occurs at t = 5.0 and 5.11s.

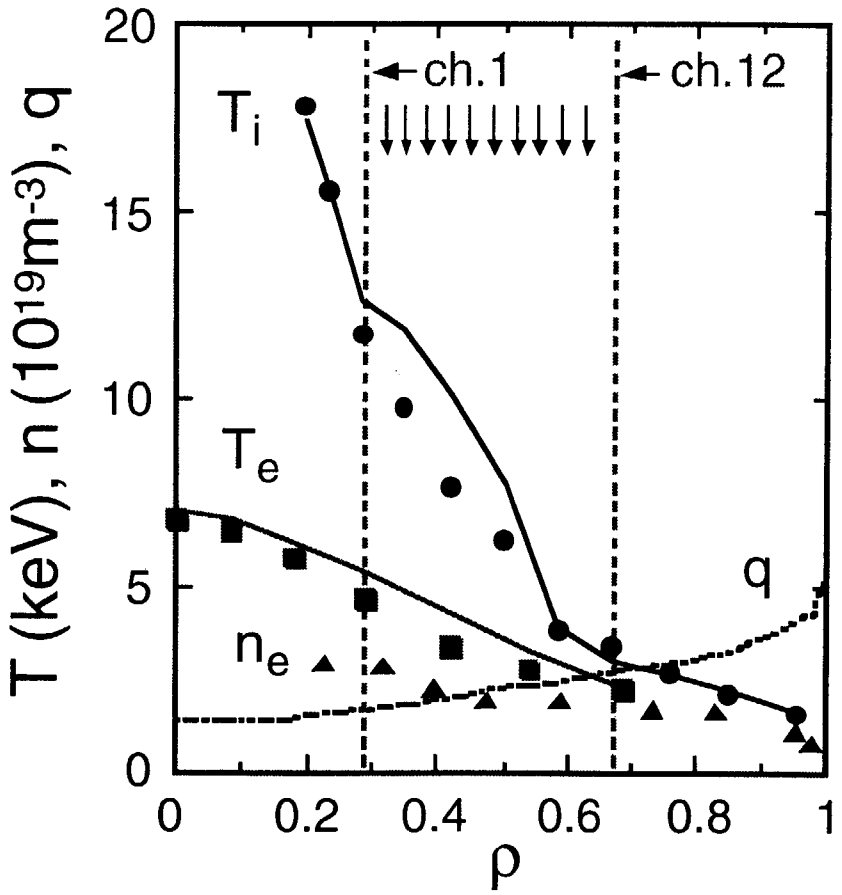

Fig. 3 Radial profiles of T_i (circles), T_e (squares), n_e (triangles), q (dotted line) just before ITB-event I at t = 4.6s. Profiles of T_i and T_e 90 ms after ITB-event I are shown by solid lines. Fast time scale evolution of T_e is measured by an ECE heterodyne radiometer with 12 channels inside the region $0.29 \leq \rho \leq 0.67$ between the two vertical dashed lines.

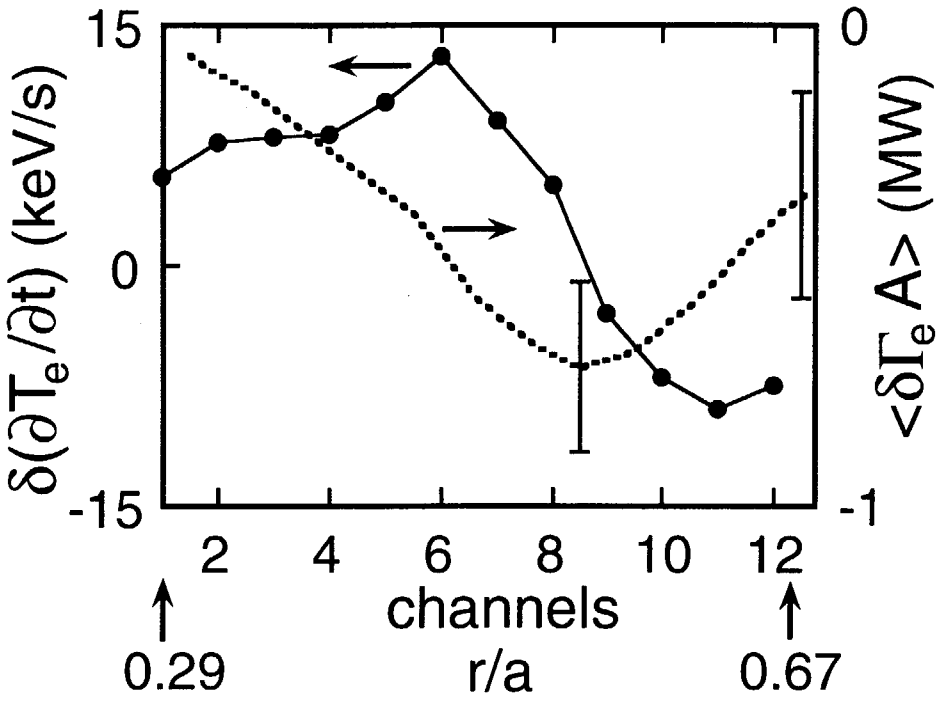

Fig. 4 Profile of $<\delta\Gamma_e A>$ (dotted line) calculated from $<\delta(\partial T_e/\partial t)>$ (circles) for ITB-event I.

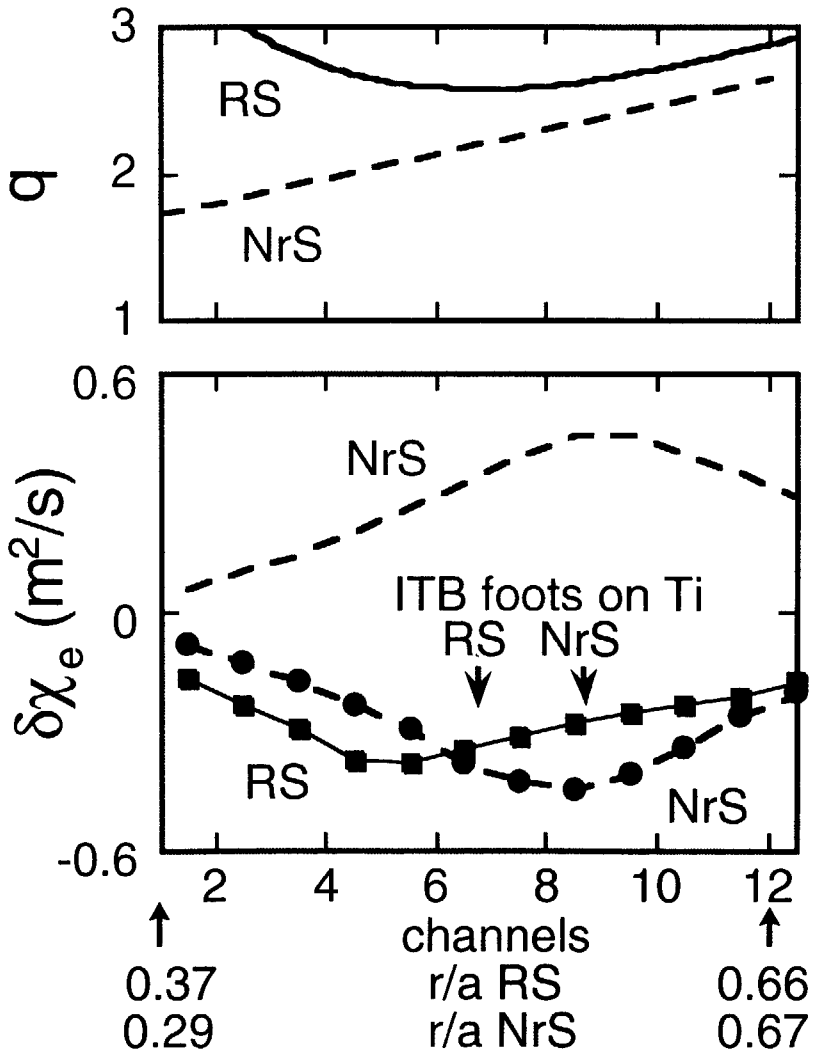

Fig. 5 Profiles of $\delta\chi_e$ at ITB-events in NrS and RS plasmas with weak ITBs: circles for ITB-event I (calculated from $<\delta(\partial T_e/\partial t)>$ shown in Fig. 4) and dashed line for ITB-event D in shot 34487; RS- solid line, shot 32423; positions of radiometer ch.1-12 are from r/a = 0.37 to 0.66 in RS and from r/a = 0.29 to 0.67 in NrS. Profiles of q are shown by solid line for RS and dashed line for NrS plasmas.

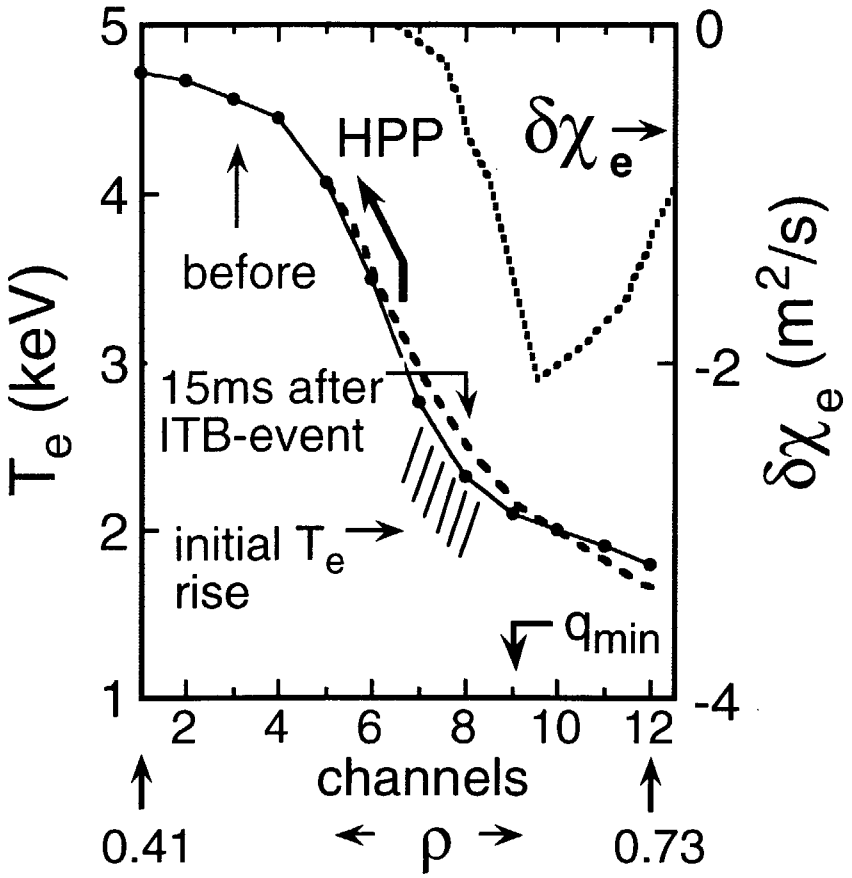

Fig. 6 Profiles of T_e before (time A in Fig. 13) and 15ms after (time B in Fig. 13) ITB-event in RS plasmas with strong ITB in shot 32424, region of inward HPP created by rise of T_e at radiometer channels 7,8 (described in Section 3) is shown by arrow HPP. Profile of $\delta\chi_e$ is shown by dotted line.

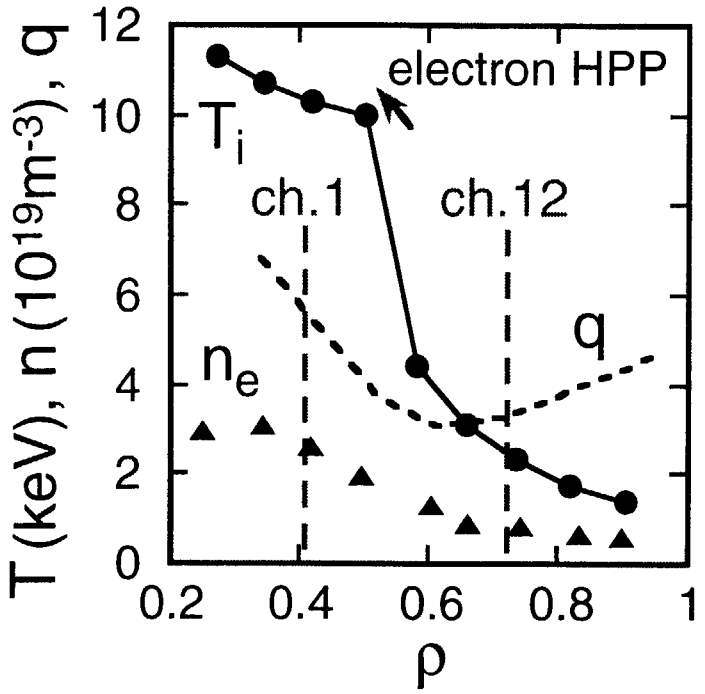

Fig. 7 Radial profiles of T_i (circles), n_e (triangles) and q (dashed line) before ITB-event in Fig. 6, arrow HPP- the same region as in Fig. 6.

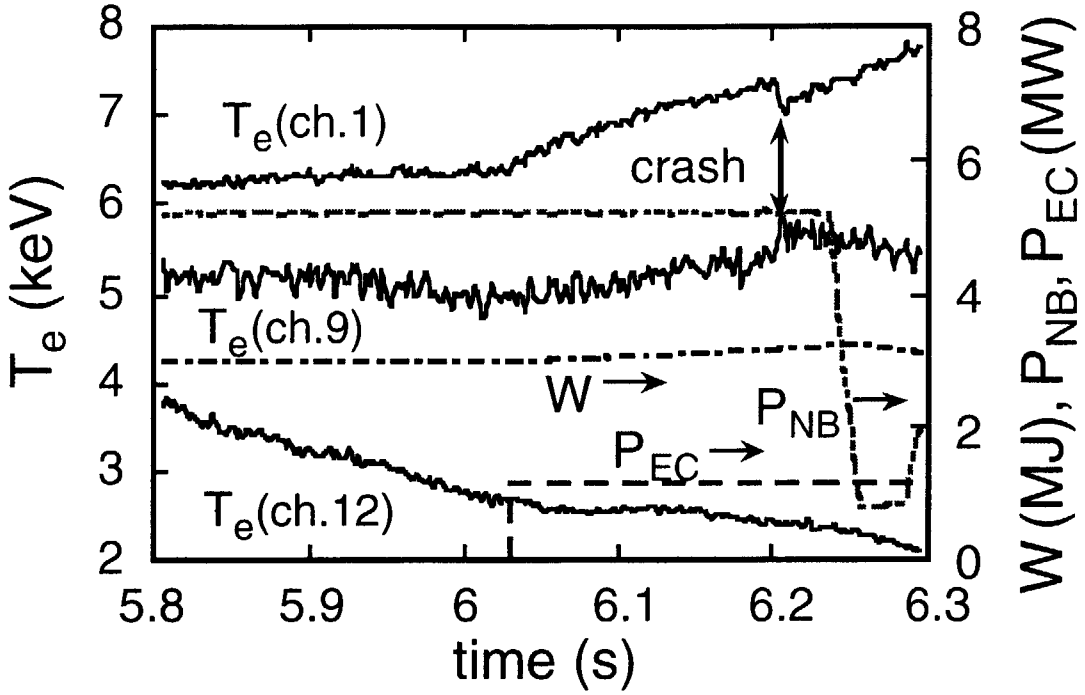

Fig. 8 Evolutions of W, P_{NB}, P_{EC} and T_e(ch.1,9,12) for the RS discharge 36614 with strong ITB. The sawtooth-like crash at t = 6.203s is shown by the arrow. Temperatures are measured at ρ = 0.3,0.53,0.62.

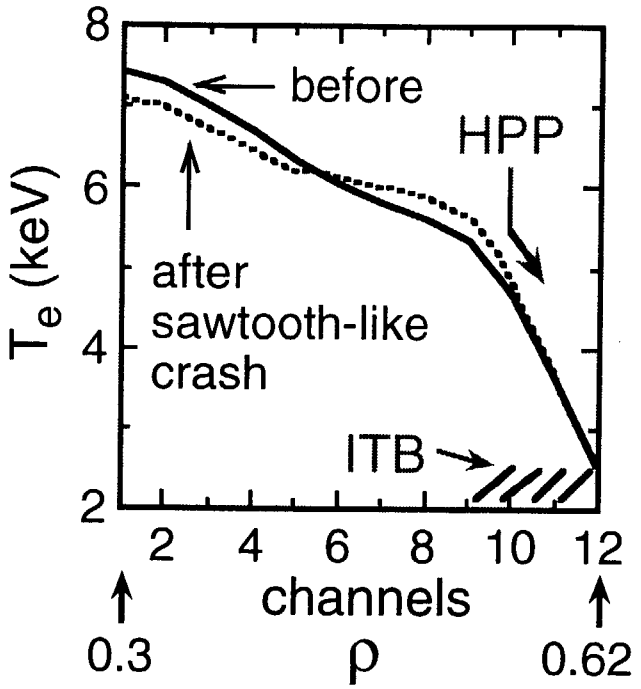

Fig. 9 Profiles of T_e measured by radiometer before (solid line) and after (dotted line) sawteeth-like crash (see the arrow "crash" at t = 6.203s in Fig. 8). The region of crash-induced outward HPP in the ITB is shown by the arrow "HPP".

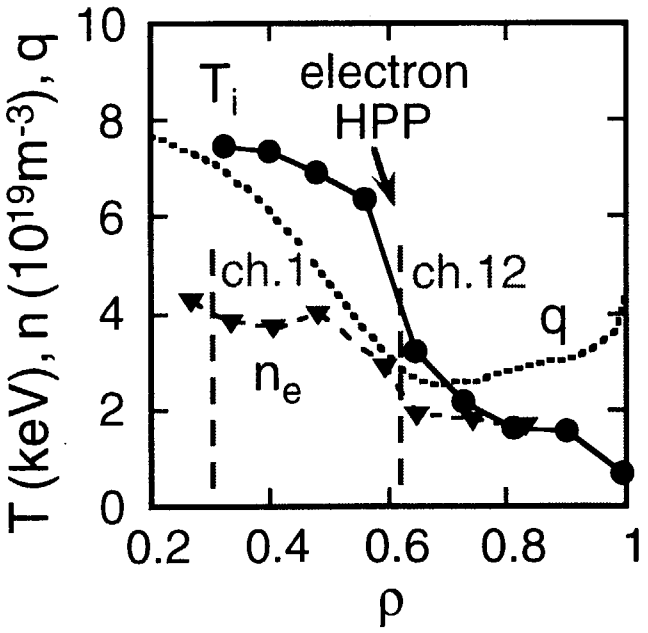

Fig. 10 Profiles of T_i (circles), n_e (triangles) and q (dotted line) before sawtooth-like crash in shot 36614. The region of electron HPP is shown by the arrow.

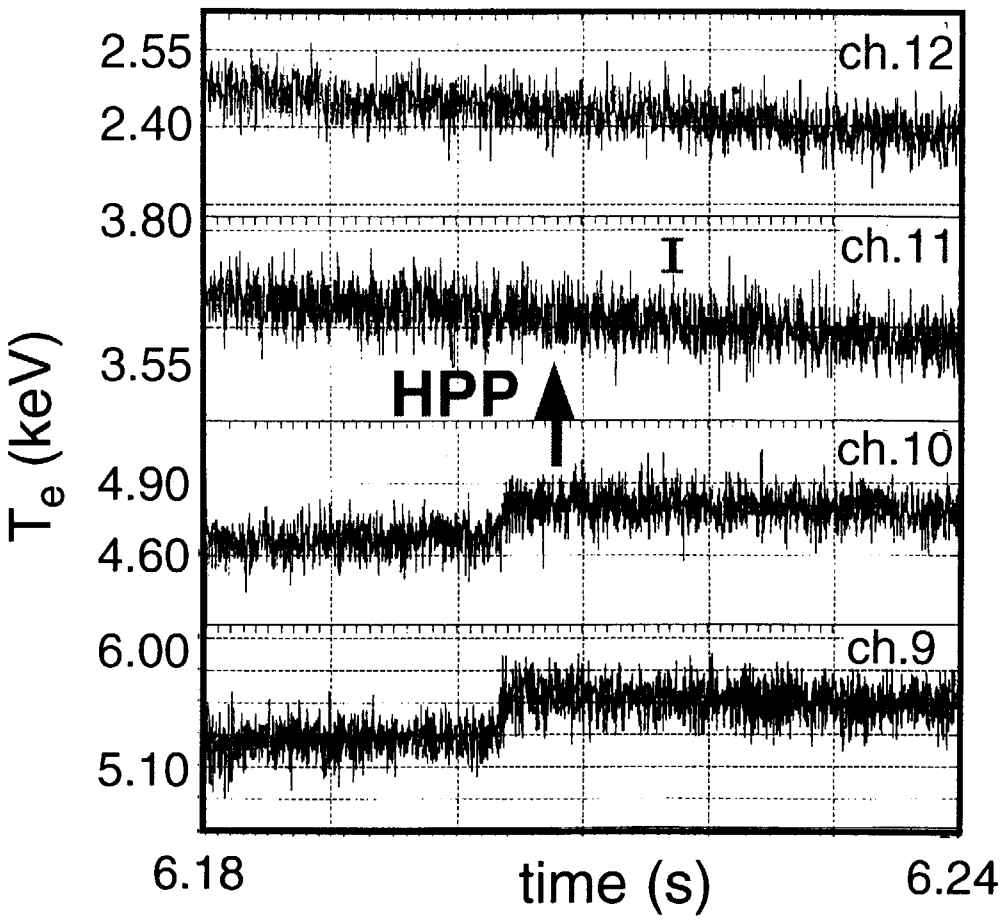

Fig. 11 Evolution of T_e for shot 36614. Crash-induced outward HPP from radiometer channel 10 to channel 11 is not seen. The T_e perturbation on channel 11 calculated with $\chi_e^{HP} = 0.1 m^2/s$ (15ms after the crash, see Fig. 12) is shown by short segment of vertical line.

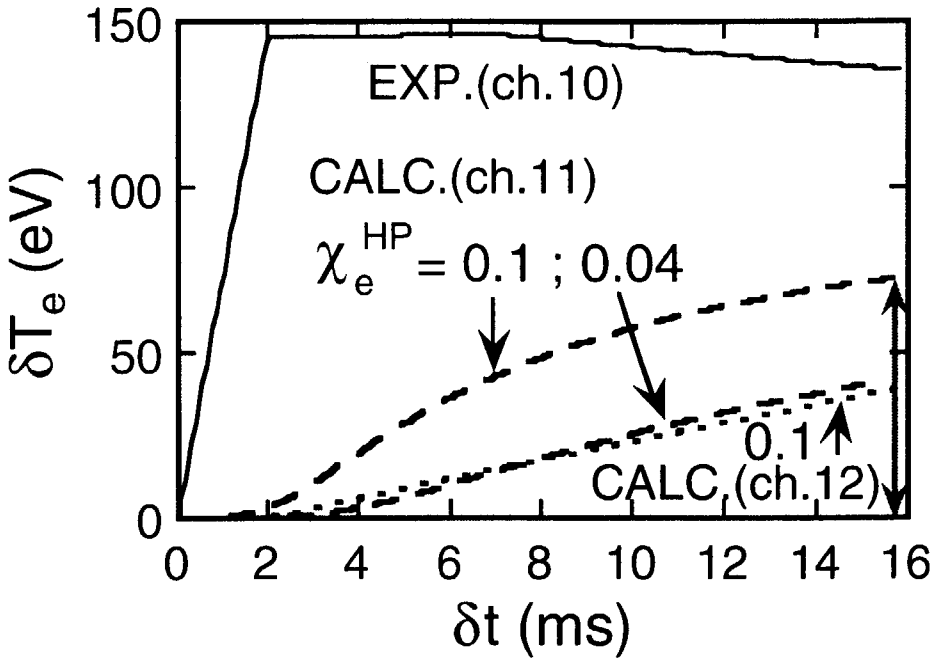

Fig. 12 Calculations of HPP from radiometer channel 10 to channels 11 and 12. Experimental $\delta T_{e,EXP}(r_{10},t)$ is shown by solid line and calculated $\delta T_{e,CALC}(r_{11},t)$ with χ_e^{HP}=0.1 and 0.04 m^2/s shown by dashed lines. Evolution of $\delta T_{e,CALC}(r_{12},t)$ with χ_e^{HP} = 0.1m^2/s is shown by dotted line. The perturbation $\delta T_{e,CALC}(r_{11},t=t_{CRASH}$ + 15ms) with χ_e^{HP} = 0.1m^2/s is shown by double-side arrow (this value is shown by short segment of vertical line in Fig.11).

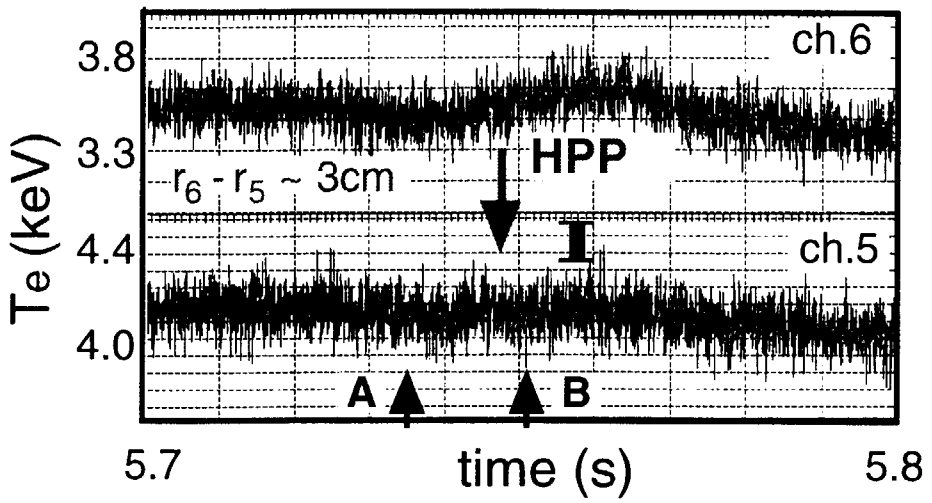

Fig. 13 ITB-event induced inward HPP from radiometer channel 6 to channel 5 inside strong ITB in shot 32424. Profiles of T_e at the time A (just before ITB-event) and 15ms later at the time B are shown in Fig. 6. The calculated perturbation of T_e at channel 5 with $\chi_e^{HP} = 0.2m^2/s$ (26ms after time A) is shown by bold segment.

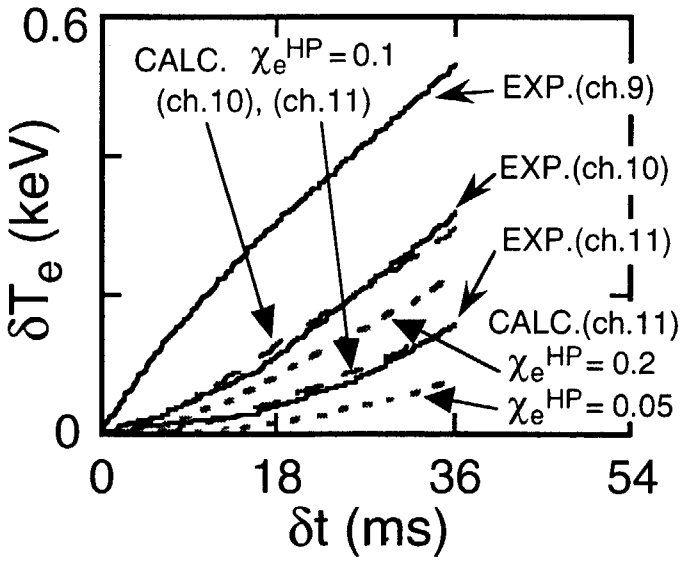

Fig. 14 ITB-event induced outward HPP from radiometer channel 9 to channels 10 and 11 inside ITB in positive shear region of RS plasmas in shot E32423. Comparison of $\delta T_{e,EXP}(r_{9,10,11},t)$ (solid lines) and $\delta T_{e,CALC}(r_{10,11},t)$ with $\chi_e^{HP} = 0.1 m^2/s$ (dashed lines) is shown. Evolutions of $\delta T_{e,CALC}$ (r_{11},t) with $\chi_e^{HP} = 0.2$ and 0.05 m^2/s are drawn by dotted lines.

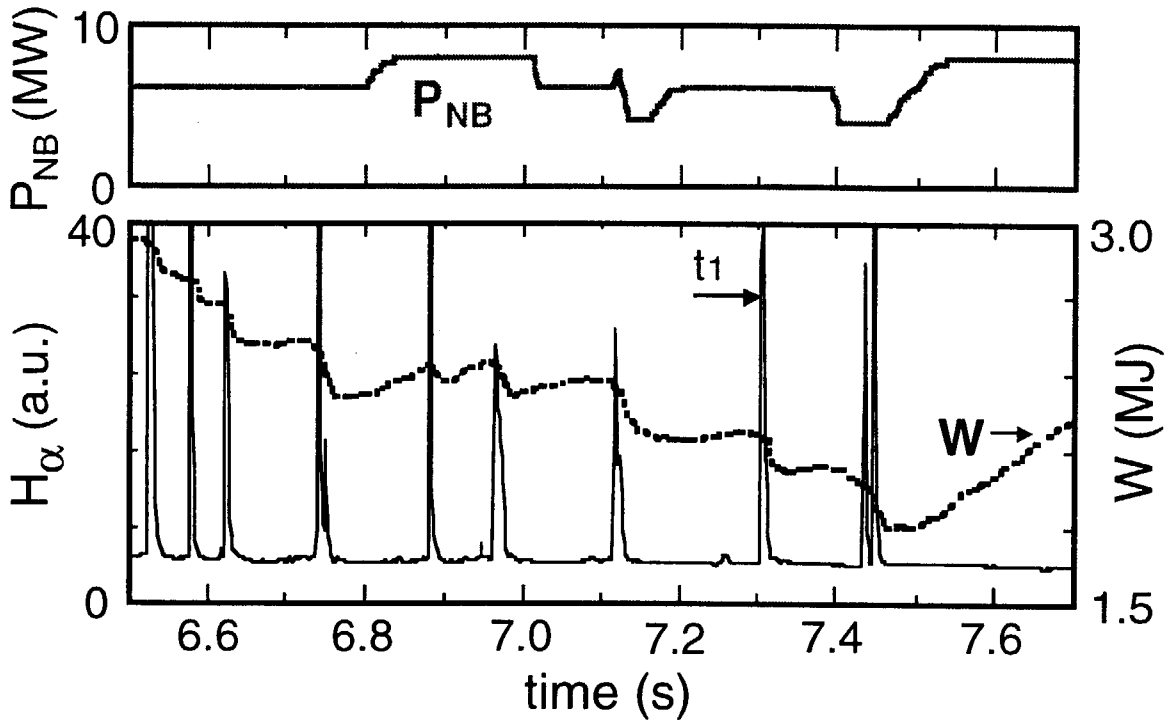

Fig. 15 Time traces of H_α, W, P_{NB} in RS shot 32419. ELM shown by arrow t_1 is studied in detail below.

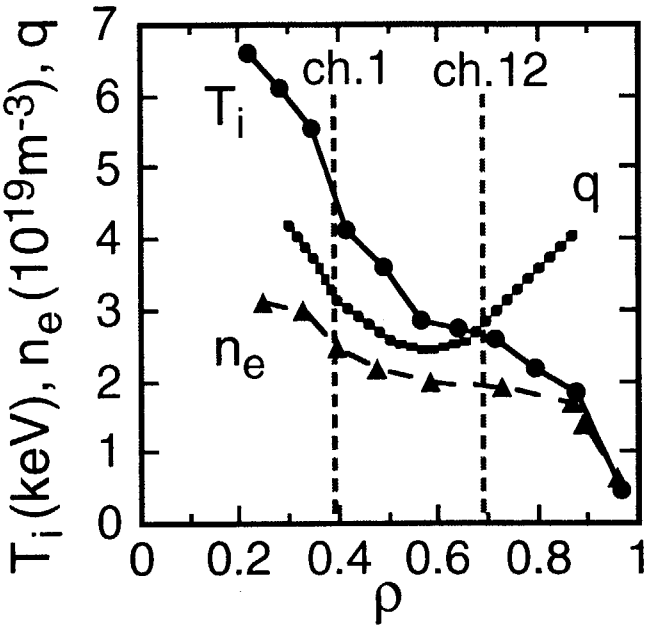

Fig. 16 Radial profiles of T_i (circles), n_e (triangles), q (dotted line) before ELM at $t = t_1$. Location of radiometer channels 1 and 12 is shown by vertical dashed lines.

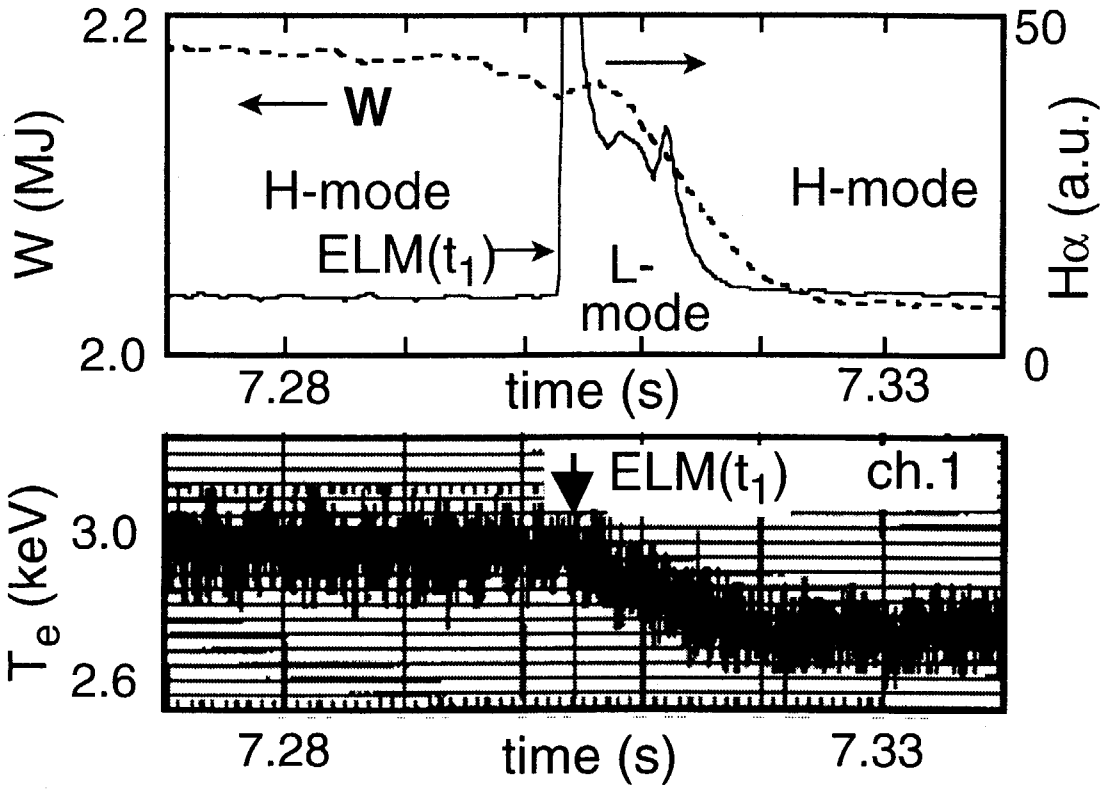

Fig. 17 Time traces of W, H_α and T_e measured on radiometer channel 1 around ELM at $t = t_1$. Fast response of T_e(ch.1) to H-L and L-H transitions is seen.

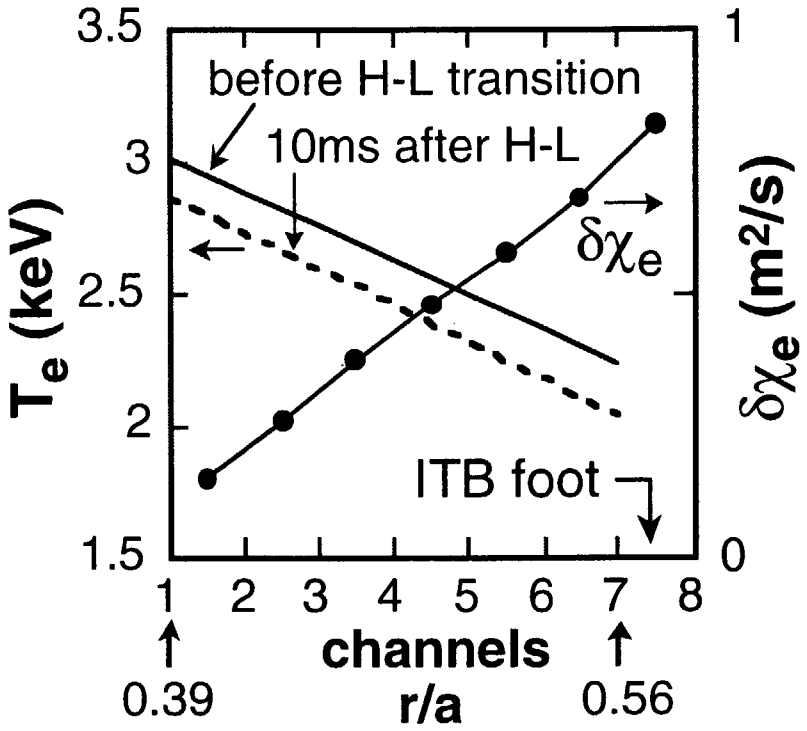

Fig. 18 T_e profiles before (solid line) and 10ms after (dashed line) the H-L transition at $t = t_1$, together with the χ_e change (circles).

国際単位系(SI)と換算表

表1　SI基本単位および補助単位

量	名称	記号
長さ	メートル	m
質量	キログラム	kg
時間	秒	s
電流	アンペア	A
熱力学温度	ケルビン	K
物質量	モル	mol
光度	カンデラ	cd
平面角	ラジアン	rad
立体角	ステラジアン	sr

表2　SIと併用される単位

名称	記号
分，時，日	min，h，d
度，分，秒	°，′，″
リットル	l，L
トン	t
電子ボルト	eV
原子質量単位	u

1 eV = 1.60218 × 10^{-19} J

1 u = 1.66054 × 10^{-27} kg

表3　固有の名称をもつSI組立単位

量	名称	記号	他のSI単位による表現
周波数	ヘルツ	Hz	s^{-1}
力	ニュートン	N	m·kg/s^2
圧力，応力	パスカル	Pa	N/m^2
エネルギー，仕事，熱量	ジュール	J	N·m
工率，放射束	ワット	W	J/s
電気量，電荷	クーロン	C	A·s
電位，電圧，起電力	ボルト	V	W/A
静電容量	ファラド	F	C/V
電気抵抗	オーム	Ω	V/A
コンダクタンス	ジーメンス	S	A/V
磁束	ウェーバ	Wb	V·s
磁束密度	テスラ	T	Wb/m^2
インダクタンス	ヘンリー	H	Wb/A
セルシウス温度	セルシウス度	℃	
光束	ルーメン	lm	cd·sr
照度	ルクス	lx	lm/m^2
放射能	ベクレル	Bq	s^{-1}
吸収線量	グレイ	Gy	J/kg
線量当量	シーベルト	Sv	J/kg

表4　SIと共に暫定的に維持される単位

名称	記号
オングストローム	Å
バーン	b
バール	bar
ガル	Gal
キュリー	Ci
レントゲン	R
ラド	rad
レム	rem

1 Å = 0.1 nm = 10^{-10} m

1 b = 100 fm^2 = 10^{-28} m^2

1 bar = 0.1 MPa = 10^5 Pa

1 Gal = 1 cm/s^2 = 10^{-2} m/s^2

1 Ci = 3.7 × 10^{10} Bq

1 R = 2.58 × 10^{-4} C/kg

1 rad = 1 cGy = 10^{-2} Gy

1 rem = 1 cSv = 10^{-2} Sv

表5　SI接頭語

倍数	接頭語	記号
10^{18}	エクサ	E
10^{15}	ペタ	P
10^{12}	テラ	T
10^{9}	ギガ	G
10^{6}	メガ	M
10^{3}	キロ	k
10^{2}	ヘクト	h
10^{1}	デカ	da
10^{-1}	デシ	d
10^{-2}	センチ	c
10^{-3}	ミリ	m
10^{-6}	マイクロ	μ
10^{-9}	ナノ	n
10^{-12}	ピコ	p
10^{-15}	フェムト	f
10^{-18}	アト	a

（注）

1. 表1　5は「国際単位系」第5版，国際度量衡局　1985年刊行による。ただし，1 eVおよび1 uの値はCODATAの1986年推奨値によった。
2. 表4には海里，ノット，アール，ヘクタールも含まれているが日常の単位なのでここでは省略した。
3. barは，JISでは流体の圧力を表わす場合に限り表2のカテゴリーに分類されている。
4. EC閣僚理事会指令ではbar，barnおよび「血圧の単位」mmHgを表2のカテゴリーに入れている。

換　算　表

力	N(=10^5 dyn)	kgf	lbf
	1	0.101972	0.224809
	9.80665	1	2.20462
	4.44822	0.453592	1

粘度　1 Pa·s(N·s/m^2) = 10 P(ポアズ)(g/(cm·s))

動粘度　1 m^2/s = 10^4 St(ストークス)(cm^2/s)

圧力	MPa(=10 bar)	kgf/cm^2	atm	mmHg(Torr)	lbf/in^2(psi)
	1	10.1972	9.86923	7.50062 × 10^3	145.038
	0.0980665	1	0.967841	735.559	14.2233
	0.101325	1.03323	1	760	14.6959
	1.33322 × 10^{-4}	1.35951 × 10^{-3}	1.31579 × 10^{-3}	1	1.93368 × 10^{-2}
	6.89476 × 10^{-3}	7.03070 × 10^{-2}	6.80460 × 10^{-2}	51.7149	1

エネルギー・仕事・熱量	J(=10^7 erg)	kgf·m	kW·h	cal(計量法)	Btu	ft·lbf	eV
	1	0.101972	2.77778 × 10^{-7}	0.238889	9.47813 × 10^{-4}	0.737562	6.24150 × 10^{18}
	9.80665	1	2.72407 × 10^{-6}	2.34270	9.29487 × 10^{-3}	7.23301	6.12082 × 10^{19}
	3.6 × 10^6	3.67098 × 10^5	1	8.59999 × 10^5	3412.13	2.65522 × 10^6	2.24694 × 10^{25}
	4.18605	0.426858	1.16279 × 10^{-6}	1	3.96759 × 10^{-3}	3.08747	2.61272 × 10^{19}
	1055.06	107.586	2.93072 × 10^{-4}	252.042	1	778.172	6.58515 × 10^{21}
	1.35582	0.138255	3.76616 × 10^{-7}	0.323890	1.28506 × 10^{-3}	1	8.46233 × 10^{18}
	1.60218 × 10^{-19}	1.63377 × 10^{-20}	4.45050 × 10^{-26}	3.82743 × 10^{-20}	1.51857 × 10^{-22}	1.18171 × 10^{-19}	1

1 cal = 4.18605 J(計量法)

= 4.184 J　(熱化学)

= 4.1855 J　(15 °C)

= 4.1868 J(国際蒸気表)

仕事率　1 PS(仏馬力)

= 75 kgf·m/s

= 735.499 W

放射能	Bq	Ci
	1	2.70270 × 10^{-11}
	3.7 × 10^{10}	1

吸収線量	Gy	rad
	1	100
	0.01	1

照射線量	C/kg	R
	1	3876
	2.58 × 10^{-4}	1

線量当量	Sv	rem
	1	100
	0.01	1

（86年12月26日現在）

Dynamic Behavior of Transport in Normal and Reversed Shear Plasmas with Internal Barriers in JT-60U